First-principles studies of Ta_2O_5 polymorphs

Yu-Ning Wu, Lan Li, and Hai-Ping Cheng
Quantum Theory Project and Department of Physics, University of Florida, Gainesville Florida 32611, USA
(Received 8 June 2009; revised manuscript received 22 November 2010; published 14 April 2011)

Using density functional theory (DFT) with generalized gradient approximations (GGA) and the projector-augmented wave method, we have investigated the structure, energetics, elastic tensors, and mechanical properties of four crystalline forms of Ta_2O_5 with exact stoichiometry as well as a model amorphous structure. We have also constructed a virtual crystal potential to address partial oxygen occupancy and compared it to models of explicit oxygen vacancies and of the oxygen-rich system. Our calculations show that mechanical properties of these polymorphs are highly anisotropic. By comparison with experimental data, we find that all crystalline phases and the simulated amorphous phase have a Young's modulus higher than the amorphous thin film that is probed experimentally, but the variation among crystalline structures is as high as a factor of 2. Electronic properties of three Ta_2O_5 polymorphs have been calculated using a hybrid DFT and explicit exchange functional method that improves the gap size compared to that obtained by GGA. We suggest that further experimental measurements on tantala crystals are needed to understand the physical properties of this important material.

DOI: 10.1103/PhysRevB.83.144105 PACS number(s): 62.20.−x, 68.60.Bs, 87.16.A−, 61.50.−f

I. INTRODUCTION

Tantalum pentoxide (Ta_2O_5),[1] or tantala, is a potential alternative to SiO_2 because of its high breakdown voltage, high dielectric constant,[2] and excellent step coverage characteristics.[3] In addition to its applications as dielectric films,[4] this material also has been used experimentally for optical coatings[5] and corrosion coatings.[6] The inspiration for the work in this paper arises from the need for optical coatings in ultraprecision measurements. In ongoing experiments conducted by the laser interferometer gravitational observatory (LIGO), alternating layers of SiO_2 and Ta_2O_5 are used as coatings for the test masses in gravitational wave detectors. It is predicted that the limiting noise in wave detection will be the thermal noise that is closely related to mechanical dissipation and properties of the coating materials.[7,8] For the SiO_2/Ta_2O_5 coatings studied, the mechanical dissipation appears to be associated with the Ta_2O_5 component of the coatings.[9] In addition, the film elastic properties of SiO_2/Ta_2O_5 coatings can significantly influence the expected level of coating thermal noise.[7] The structural and mechanical properties of Ta_2O_5 films are thus of considerable importance.

Tantala has many crystalline forms, including those which are oxygen rich and oxygen deficient. A phase transformation in pure bulk Ta_2O_5 at ∼1360 °C was reported[10] a long time ago, but the nature of the structure for each phase continued to stimulate research activity. At low temperature, various polymorphs have been proposed because of the difficulty in growing single-crystal low-temperature form Ta_2O_5 (L-Ta_2O_5) using conventional high-temperature techniques. A variety of L-Ta_2O_5 structures can be stabilized by adding certain amounts of other oxides.[11–17] The first one was reported by Stephenson *et al.*[16] in 1971. The group used the x-ray powder diffraction method and proposed a crystal structure with an orthorhombic unit cell that consists of 22 Ta and 55 O atoms with a large number of oxygen vacancies. Those were then identified as the main cause for a large leakage current.[18] In a later study, a vacancy-free L-Ta_2O_5 orthorhombic structure (β-Ta_2O_5) which contains only four tantalum and ten oxygen atoms in the unit cell was observed via x-ray diffraction,[11] and verified by calculations using density functional theory within the local-density approximation (LDA) and generalized gradient approximation (GGA).[19] Besides β-Ta_2O_5, researchers also had reported a hexagonal structure for the low-temperature phase of Ta_2O_5 (δ-Ta_2O_5).[20] Fukumoto *et al.*[21] studied the crystal structure of hexagonal Ta_2O_5, which has the space group of *P*6/*mmm*, using first-principles ultrasoft pseudopotential calculations. Interestingly, a very recent first-principles study[22] showed that both β-Ta_2O_5 and δ-Ta_2O_5 show some instability and large supercells were used to optimize structure.

For the high-temperature form of Ta_2O_5 (H-Ta_2O_5), orthorhombic, tetragonal, and monoclinic models have been proposed.[17,23,24] Similar to L-Ta_2O_5, single-crystal H-Ta_2O_5 can be grown with the help of other oxides. Two types of modulations have been proposed for TiO_2-stabilized H-Ta_2O_5. One was determined by Liu *et al.*[25] in 2006 using the conventional solid-state reaction method and the advanced laser irradiation technique to hold the pure H-Ta_2O_5 structure at room temperature. They identified the tetragonal structure of pure Ta_2O_5 with the space group of *I*41/*amd* using transmission electron microscopy (TEM). For the second high-temperature tantala, Makovec *et al.*[26] constructed a complicated structural model from the analysis of the electron diffraction data and high-resolution electron microscopy (HREM) electron images of the solid solutions in the series $(1-x)Ta_2O_5$-$xTiO_2$ with $x = 0.0$–0.1. The proposed monoclinic crystalline structure is based on edge sharing of an oxygen octahedron-hexagonal bipyramid-octahedron molecule building block. This unit block repeats four times in a unit cell of high temperature of Ta_2O_5.

So far, experimental information is mostly limited to structure determination. Crystal-structure-specific mechanical and optical properties are yet to be determined. Compared to the experimental work on Ta_2O_5 mentioned above, theoretical efforts, in particular for the high-temperature phases of Ta_2O_5, is even further far behind. We will see later that even the low-temperature phases are not well understood. In this paper, we present our theoretical results on tantala

starting with the two relatively simple, low-temperature Ta_2O_5 polymorphs and followed by a high-temperature structure and a complicated low-temperature structure. Both have partial oxygen occupation issues that have been studied using the virtual crystal approximation (VCA).[27] In addition, we present our results for a model amorphous structure.

The rest of the paper is organized as follows: In Sec. II, we discuss theoretical methods. In Sec. III, we present our results on structures (Sec. III A), cohesive energy and density of states (Sec. III B), and elastic moduli (Sec. III C), and finally, in Sec. IV, we discuss and conclude our investigations.

II. COMPUTATIONAL METHODS

Our structural and mechanical calculations were performed using the plane-wave Vienna *Ab-initio* Simulation Program (VASP) code[28–30] based on self-consistent density functional theory (DFT).[31] We used projector-augmented wave potentials (PAWs)[32,33] in conjunction with plane-wave expansion. The exchange and correlation potentials were calculated using the generalized gradient approximation (GGA) with Perdew-Wang 91 parametrization (PW91).[34] The energy cutoff was 520 eV for wave functions. A Gaussian smearing of 0.1 eV was used for the Fermi-surface broadening. Surface Brillouin-zone integrations were performed on a Monkhorst-Pack[35] k mesh of $8 \times 8 \times 8$ in the Methfessel-Paxton scheme[36] for two low-temperature crystal structures of Ta_2O_5, as well as $8 \times 8 \times 1$ for the high-temperature structure of Ta_2O_5. With these k meshes, the total energies are converged to 0.01 eV. The equilibrium lattice constants for different Ta_2O_5 structures were obtained through total energy minimization. The force tolerance for geometry relaxation was 0.02 eV/Å. For electronic properties, the HSE06 hybrid exchange correlation[37,38] also was used to calculate the density of states and for comparison with results obtained from PW91.

To simulate systems with partially occupied sites, we constructed pseudopotentials within the framework of VCA.[27] In VCA, partially occupied sites are assumed to be fully occupied by pseudoatoms with the pseudopotential modified by occupancy. Without VCA, many possible configurations can be generated and hence a large supercell is needed to investigate the system.

In the equilibrium state, the cohesive energy is calculated as

$$E_c = (E_{\text{total}} - n_{\text{Ta}}E_{\text{Ta}} - n_{\text{O}}E_{\text{O}})/(n_{\text{Ta}} + n_{\text{O}}), \tag{1}$$

where E_{total} is the total energy per cell of a configuration. n_A specifies the number of a particular element ($A = \text{Ta, O}$) in that unit cell, and E_A ($A = \text{Ta, O}$) is the energy of an individual atom calculated with spin-dependent DFT.

Elastic properties can be obtained by calculating the elastic tensor c_{ij}, which relates the stress with the strain for a given system,[39] that is,

$$\sigma_i = \text{sum}_{j=1,6} c_{ij}\varepsilon_j, \tag{2}$$

where σ_i are stress components and ε_j are small strains. We used the *ab initio* calculation to relate stress response to strains, and elastic constants can be obtained by solving a set of linear equations of c_{ij}.[40] For all crystalline systems we studied, 1.5% strain is added in six strains ($\varepsilon_1 - \varepsilon_6$). To obtain sufficiently accurate elastic constants, we adopted stricter convergence and relaxation criteria than the ones used for total energy determination. The force tolerance in relaxation in this study is set to 0.01 eV/Å, and the stress values vary less than 0.02 kbar.

The number of independent elastic constants varies depending on crystalline symmetry. In the case of orthorhombic β-Ta_2O_5, nine independent elastic constants are involved according to Ravindran *et al.*[41] Both of the polycrystalline bulk modulus (B) and shear modulus (G) can be determined based on c_{ij}. Two methods, Voigt approximation[42] (index V) and Reuss approximation[43] (index R), were proposed. Hill[44] proved that these two methods correspond to upper and lower bounds of the true polycrystalline elastic constants. An approximation can be made by taking average of Voigt and Reuss method results,

$$G = \tfrac{1}{2}(G_{\text{R}} + G_{\text{V}}) \quad \text{and} \quad B = \tfrac{1}{2}(B_{\text{R}} + B_{\text{V}}). \tag{3}$$

The average Young's modulus Y and Poisson's ratio ν can be determined by

$$Y = \frac{9BG}{3B + G} \quad \text{and} \quad \upsilon = \frac{3B - 2G}{2(3B + G)}. \tag{4}$$

Reuss moduli (G_R and B_R) and Voigt moduli (G_V and B_V) are written as[41]

$$B_{\text{R}} = \frac{1}{(s_{11} + s_{22} + s_{33}) + 2(s_{12} + s_{13} + s_{23})}, \tag{5}$$

$$B_{\text{V}} = \frac{1}{9}(c_{11} + c_{22} + c_{33}) + \frac{2}{9}(c_{12} + c_{13} + c_{23}), \tag{6}$$

$$G_{\text{R}} = \frac{15}{4(s_{11}+s_{22}+s_{33})-4(s_{12}+s_{13}+s_{23})+3(s_{44}+s_{55}+s_{66})}, \tag{7}$$

$$G_{\text{V}} = \frac{1}{15}(c_{11} + c_{22} + c_{33} - c_{12} - c_{13} - c_{23}) + \frac{1}{5}(c_{44} + c_{55} + c_{66}), \tag{8}$$

where s_{ij} are the elastic compliance constants, and s is the inverse of the elastic tensor c.

The directional dependence of Young's modulus in an orthorhombic crystal can be calculated by[45]

$$Y = \frac{1}{\left(l_1^4 s_{11} + l_2^4 s_{22} + l_3^4 s_{33} + 2l_1^2 l_2^2 s_{12} + 2l_2^2 l_3^2 s_{23} + 2l_1^2 l_3^2 s_{23} + l_1^2 l_2^2 s_{66} + l_1^2 l_3^2 s_{55} + l_2^2 l_3^2 s_{44}\right)}, \tag{9}$$

where l_i's are direction cosines to x, y, z, and s_{ij}'s are the elastic compliance constants. Young's modulus along axis i then becomes

$$Y_i = \frac{1}{s_{ii}}, \tag{10}$$

where i can be 1, 2, or 3.

For some systems, we have also computed directly the bulk modulus according to second derivative of energy as

$$B = -V_0 \frac{d^2E}{dV^2}, \tag{11}$$

where V_0 is the volume in the equilibrium state, and d^2E/dV^2 denotes the second derivative of energy with respect to volume. Young's modulus and Poisson's ratio are

$$Y = \left(\frac{L_0}{A_0}\right)\frac{d^2E}{dL^2}, \tag{12}$$

$$\nu = -\frac{1}{2}\frac{L_0}{A_0}\frac{dA}{dL}, \tag{13}$$

where L_0 is the original length of the material. A_0 is the original cross-sectional area though which the force is applied. d^2E/dL^2 denotes the second derivative of the energy with respect to length. Comparison of the direct approach and approximated approach are made for some (001) direction to confirm our results.

The primary reason for performing the direct calculations is to check the validity of the VCA. The value of modulii and Poisson ratio from Eqs. (11)–(13) are different from the ones from Eqs. (2)–(10) because of some constraints applied during calculations. To obtain mechanical properties, one should use Eqs. (2)–(10).

III. RESULTS AND DISCUSSION

A. Structures

This section presents the four equilibrium structures of low- and high-temperature tantala. In addition, an amorphous model is also discussed in this part.

1. δ and β L-Ta_2O_5

The two low-temperature structures are δ-Ta_2O_5 and β-Ta_2O_5, which crystallize in a hexagonal structure and an orthorhombic structure, respectively [see Figs. 1(a) and 1(b)]. Both of them contain four tantalum and ten oxygen atoms per cell; thus the Ta:O ratio is 2:5. The experimentally reported space groups are *p6/mmm* for the δ phase and *pccm* for the β phase, respectively. However, the optimized structures show large distortions when the symmetry constraint is lifted. This phenomenon was discussed in a recent work[22] where large supercells were used. Similarly, negative phonon frequencies were obtained if symmetry was kept, indicating an unstable system. After structure optimizations without the symmetry constraints, these two structures distort further and the phonon frequencies at the gamma point become positive. The optimized lattice parameters are listed in Table I. In the hexagonal structure (δ-Ta_2O_5), the optimized lattice parameters are slightly larger than the experimental values, leading to a density 4% less than the experimental value. The results with the symmetry constraint (Table I, numbers in parentheses) are comparable to the values proposed by Sahu *et al.*,[19] and the density is 2% smaller compared to experiments. Note that the calculated a and c parameters are larger than those from the experiment, but the c/a ratio from both calculations remains the same as the experimental ratio at 0.535. The fully optimized orthorhombic structure (β-Ta_2O_5) has larger lattice parameters a and b but a smaller c, compared to the experiments.[20] Calculations with symmetry constraints show better agreement with experimental data. In particular, the calculated c/a ratio agrees well, again, with the experimental value 1.25. Densities from our calculation are 4% lower than the measured values, same as in δ-Ta_2O_5. Our results do show that δ-Ta_2O_5 has higher density than β-Ta_2O_5, which is in agreement with experiment. Tables I(a) and I(b) provide detailed descriptions of the Ta-O bond length and Ta-O-Ta bond angle before and after distortion, which are depicted in Figs. 1(a) and 1(b).

2. H-Ta_2O_5

The H-Ta_2O_5 system (reported by Liu *et al.*[25]) has a tetragonal structure with lattice parameters of $a = 3.86$ Å and $c = 36.18$ Å and $I41/amd$ space group, according to selected area electron diffraction (SAED) patterns and high-resolution electron microscopy (HREM) images. There are three basis tantalum atoms and four basis oxygen atoms in a unit cell. Based on the symmetry, one can reconstruct the unit cell with 12 tantalum and 32 oxygen atoms in a unit cell (as a reference point, this structure has been studied). However, one of the four basis oxygen atom sites in the unit cell has a fractional occupancy of 75%, which makes the actual total number of oxygen atoms 30. As a result, The O/Ta ratio is still 2.5. The positions of the two missing oxygen atoms are random. To address the partial occupancy issue, we have performed a number of calculations with different approaches, including using an oxygen-rich crystal, VCA,[27] and various combinations of two selected vacancy sites. Note that we fully expect explicit vacancy models to fail completely for electronic structure characterization. However, for mechanical properties, they can provide a reference point to check the results of VCA. In it, a 0.75-factored modification of the oxygen pseudopotential has been performed and applied to eight oxygen sites where vacancy can possibly occur, so that the number of oxygen atoms is effectively 30. In Table I, the crystal without oxygen vacancies is denoted as O-rich, and two with two specific oxygen vacancies are denoted as defect_1 and defect_2, which are typical ones among 28 different combinations of vacant sites. We have fully relaxed the lattice and internal atomic positions for all four tetragonal models. Unlike the L-tantala, this H-tantala crystal does not show visible distortion from an experimentally proposed structure when oxygen sites are either 75% or 100% occupied. The optimized geometry parameters are shown in Table I and structure in Fig. 1). Both tetragonal structures, one with 32-O and the other with 30-O effectively, maintain the tetragonal unit cell, whereas the two with explicit vacancies do not. For O-rich case the optimized a and c are 3.91 and 35.82 Å, respectively, which leads to a density of

TABLE I. The optimized lattice constants, a, b, c. Numbers in parentheses are calculated with symmetry constraints. All lengths are in units of Å. (a) Comparison of bond lengths and angles of symmetric and optimized δ-phase structure. All lengths are in units of Å and angles in degree. (b) Comparison of bond lengths and angles of symmetric and optimized β-phase structure. All lengths are in units of Å and angles in degrees.

	a (Å)	b (Å)	c (Å)	Density (g/cm^3)
L-Ta_2O_5 δ phase				
Expt.	7.25		3.88	8.37
Sahu *et al.*	7.12		3.80	8.86
Ours	7.39(7.31)		3.90(3.91)	8.01(8.17)
L-Ta_2O_5 β phase				
Expt.	6.22	3.68	7.79	8.29
Sahu *et al.*	6.19	3.63	7.66	8.59
Ours	6.38(6.30)	3.82(3.72)	7.58(7.89)	7.99(7.99)
H-Ta_2O_5				
Liu *et al.*	3.86		36.18	8.23
O-rich	3.91		35.82	8.20
With VCA	3.85		37.45	7.95
Defect_1	3.85	3.96	36.23	8.02
Defect_2	3.85	3.96	36.21	8.02
77-atom L-Ta_2O_5				
Expt.	6.20	40.29	3.89	8.37
Ours	6.74	40.37	3.84	7.79
Amorphous	11.92	12.88	13.14	8.79
With VCA	11.61	11.96	12.29	6.82

(a)	Bond length (symmetric)	Bond length (distorted)
Ta1-O2	1.96	1.99
Ta2-O1	1.99	1.95
Ta2-O6	1.99	1.94
Ta2-O4	1.96	1.94
Ta3-O7	1.99	2.23
Ta4-O5	1.99	2.10
Ta4-O9	1.99	1.90
	Angle (symmetric)	Angle (distorted)
Ta2-O1-Ta3	132.8	121.4
Ta2-O6-Ta4	132.8	157.9
Ta1-O2-Ta1	122.2	145.3
Ta3-O5-Ta4	180.0	121.9
Ta3-O9-Ta4	132.8	160.8
Ta3-O7-Ta2	132.8	157.2
Ta2-O4-Ta2	180.0	164.9

(b)	Bond length (Å) (symmetric)	Bond length in (Å) (distorted)
Ta1-O5	1.84	1.93
Ta2-O1	2.14	2.19
Ta2-O2	1.98	2.19
Ta3-O7	1.94	2.18
Ta3-O8	1.96	2.19
Ta4-O6	1.93	1.85
Ta4-O9	1.93	1.95
	Angle (symmetric)	Angle (distorted)
Ta1-O5-Ta1	180.0	138.7
Ta2-O1-Ta1	122.2	112.7
Ta2-O2-Ta1	122.2	177.5
Ta2-O3-Ta3	180.0	159.2
Ta4-O6-Ta4	180.0	138.7
Ta3-O7-Ta4	122.5	107.8
Ta3-O8-Ta4	122.5	180.0
Ta1-O9-Ta4	180.0	158.7

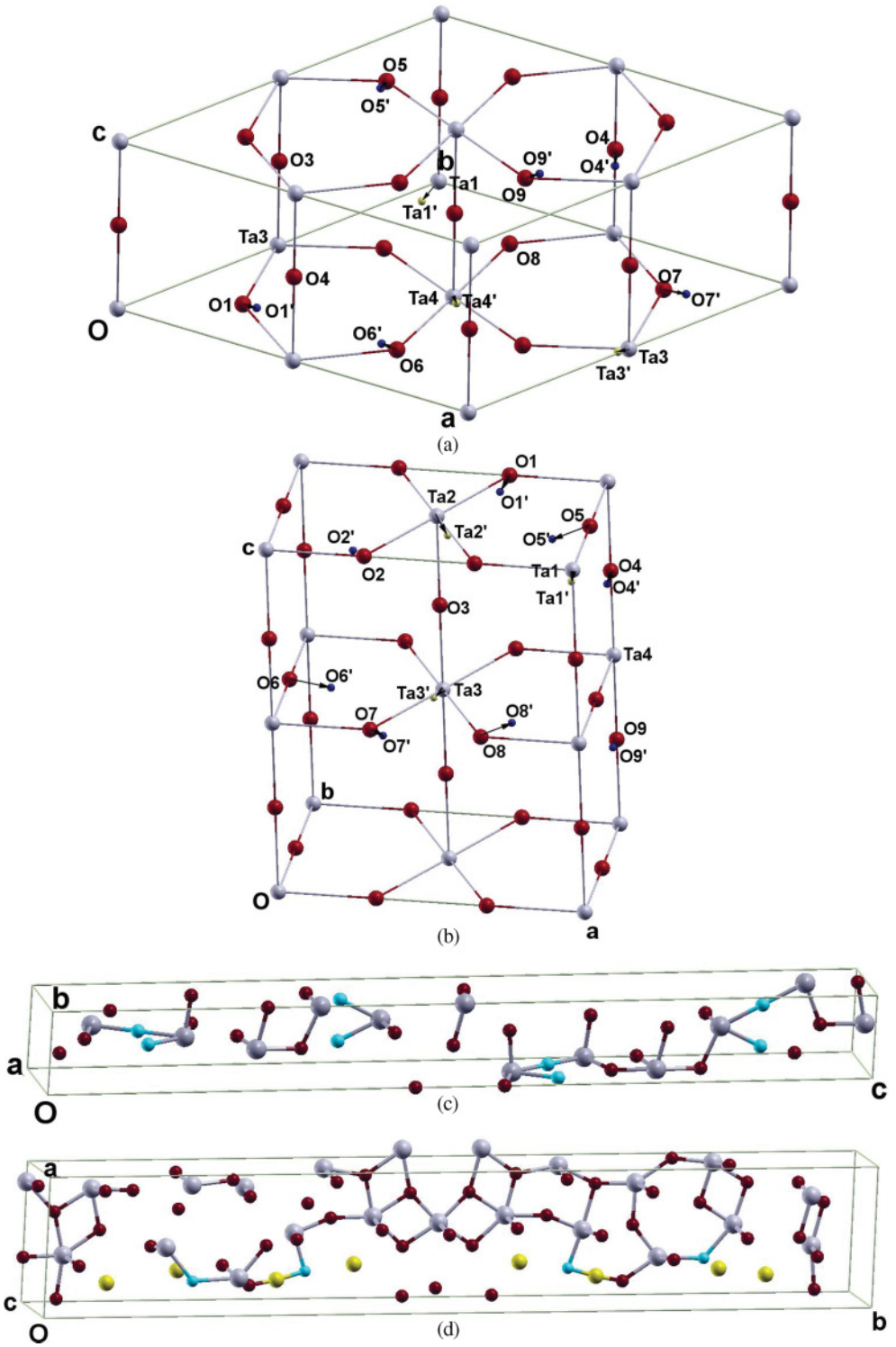

FIG. 1. (Color online) (a) Structure of δ-phase Ta_2O_5. (b) Structure of β-phase Ta_2O_5. The gray (light) atoms are Ta and red (dark) ones are oxygen. Yellow (light small) atoms are distorted Ta atoms and blue (dark small) ones are distorted oxygen atoms. Distorted atoms are labeled with primes. (c) Structure of tetragonal phase Ta_2O_5. The blue (gray) atoms are partially occupied oxygen sites. (d) Structure of low temperature phase 77-atom Ta_2O_5. Blue (gray large) are oxygen atoms with 75% occupancy and yellow (gray small) atoms are oxygen atoms with 25% occupancy.

8.20 g/cm^3 Ta_2O_5. The internal atomic coordinates do not show substantial deviation from experimental data. When VCA were used in calculations, the optimized lattice parameter a (3.85 Å) is very close to the experiment result (3.86 Å), but c is elongated that leads to a density 2.9% smaller than the measured one. Systems with two randomly selected vacancies also show lower densities than the nonvacancy O-rich model according to our calculation. This trend indicates that VCA

is not the reason of the discrepancy between calculations and experiments.

3. 77-atom L-Ta_2O_5

With the capability of VCA and reasonable test results from H-tantala, it is computationally feasible to study the W_2O_5-stablized low-temperature Ta_2O_5 phase proposed by Stephenson and Roth.[16] In the unit cell, there are 22 Ta sites and 62 O sites. However, due to oxygen vacancies, four O sites have 75% occupancy and eight O sites have 25% occupancy, which effectively makes 55 O atoms in a unit cell and keeps the Ta:O ratio as 2:5. Experimentally, the unit cell is determined as orthorhombic and the lattice constants are $a = 6.198$ Å, $b = 40.29$ Å, and $c = 3.888$ Å. For the two different occupancies of O vacancy sites, we have constructed two types of VCA potentials, 75% and 25%, respectively. After full relaxation without symmetry constraint, the orthorhombic unit cell is maintained but the lattice constants change to $a = 6.74$ Å, $b = 40.37$ Å, and $c = 3.84$ Å. The optimized unit cell is shown in Fig. 1(d). (Different vacancy sites are in different colors.) Density decreases from 8.37 to 7.79 g/cm^3 after relaxation. Similar to the H-Ta_2O_5, the symmetry of the structure is lower than for the other two L-Ta_2O_5, and the internal coordinates have also been fully relaxed without imposing any symmetry constraints.

4. Model amorphous Ta_2O_5

The last system we present in this paper is a model structure for the amorphous phase of Ta_2O_5. Because there is no published force field, we have not been able to perform a molecular dynamics calculation to obtain amorphous structures. Instead, we used a Monte Carlo method to assign positions to Ta and O atoms randomly, with constraints on the range of interatomic distance and coordination numbers. We constructed a cubic unit cell, with 48 Ta and 120 O atoms. Full structure relaxation was performed and an orthorhombic structure with lattice constants $a = 11.92$ Å, $b = 12.88$ Å, and $c = 13.14$ Å was obtained [see Fig. 2(a)]. To examine this amorphous structure, we calculated the pair correlation, which reflects radial distribution of Ta-O and Ta-Ta distances for Figs. 2(b) and 2(c). Pair correlation shows quite good amorphous characteristics, and in good agreement with experimental data.[46] However, the calculated density of this model (8.79 g/cm^3) is much higher than all other models. Therefore, we have to take oxygen vacancies into consideration.

According to Cooks *et al.*[8] and Penn *et al.*,[9] the density of Ta_2O_5 amorphous thin film ranges from 74% to 93% of bulk density, depending on different experimental conditions. The decrease in the density may come from the partial oxygen occupancy (or vacancy) in thin films (similar to the situation in the tetragonal H-Ta_2O_5). To include vacancy effects, we followed the same procedure for constructing amorphous structures, but used 80%-occupied VCA potential for oxygen atoms. In a unit cell of 32 tantalum and 100 oxygen sites, which gives effectively 80 O atoms, they were positioned randomly. After full relaxation, an 11.61 Å × 11.96 Å × 12.29 Å unit cell was obtained, with density 6.82 g/cm^3. It is 82.3% of the density of β-phase L-Ta_2O_5, within the foregoing range of 74%–93%.

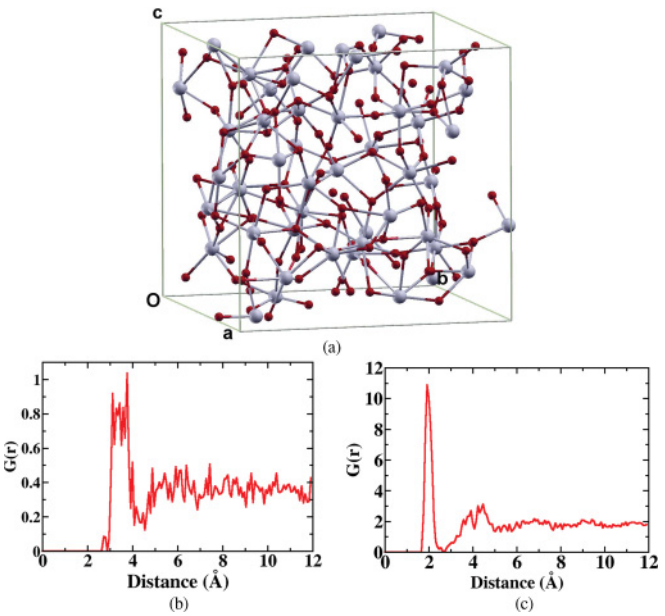

FIG. 2. (Color online) (a) Structure of amorphous Ta_2O_5. Ta atoms are in gray (light) and oxygen atoms are in red (dark). (b) Pair correlation function of Ta-Ta in a $2 \times 2 \times 2$ super cell. (c) Pair correlation function of Ta-O in a $2 \times 2 \times 2$ super cell.

B. Energetics and electronic structure

We calculated the Ta-O cohesive energies for the models mentioned above, relative to the energies of the isolated Ta and O atoms. Results are listed in Table II. Cohesive energies of the hexagonal δ-Ta_2O_5 (7.46 eV) and the orthorhombic β-Ta_2O_5 (7.41 eV) are quite similar with only a 50 meV/atom difference, indicating that the two phases are isomeric. Coincidently, the difference between the two phases seems to be the same regardless of whether or not one imposes a symmetry condition on the crystal during calculations. Our results from symmetry-constrained calculations agree with those of Sahu *et al.* For tetragonal H-Ta_2O_5, tetragonal with a VCA structure has a cohesive energy of 7.21 eV/atom, which is lower than the two L-Ta_2O_5 phases as expected. Similar to the value within VCA, the two structures each with two O vacancies both have a cohesive energy of 7.26 eV/atom, indicating that VCA is a reasonable approximation. Interestingly, the orthorhombic 77-atom L-Ta_2O_5 calculated using VCA has the

TABLE II. Numbers of oxygen and tantalum atoms, cohesive energy. Numbers in parentheses are calculated with symmetry constraints. All lengths are in units of Å.

	n_{Ta}	n_O	O/Ta	E_c (eV/atom)
L-Ta_2O_5 δ phase	4	10	2.5	7.46(7.20)
L-Ta_2O_5 β phase	4	10	2.5	7.41(7.15)
O-rich H-Ta_2O_5	12	32	2.67	7.18
With VCA	12	30	2.67	7.21
Defect_1	12	30	2.5	7.26
Defect_2	12	30	2.5	7.26
77-atom L-Ta_2O_5	22	55	2.5	7.33
168-atom amorphous	48	120	2.5	7.23
With VCA	32	80	2.5	6.77

second lowest energy, that is, 7.33 eV. Our amorphous model without vacancy shows a 7.23 eV/atom cohesive energy, which is even higher than for the tetragonal VCA model (not a surprise). However, the cohesive energy of amorphous VCA model is 6.77 eV/atom, which is lower than any other model discussed here. One should not take the exact value of this particular number too seriously, because it merely provides a clue on how the cohesive energy decreases as the systems have partially occupied oxygen sites, or equivalently, the energy decreases when there are vacancies.

The densities of state (DOS) were calculated, including δ-phase, β-phase, tetragonal H-Ta_2O_5, and the 77-atom low-T model. To obtain a sensible band gap, which is known to be underestimated by DFT with conventional LDA or GGA, we used the HSE06 hybrid functional to calculate the DOS of the first three systems. Figure 3 shows the DOS for L- and H-Ta_2O_5 structures. As shown in Figs. 3(a) and 3(b), GGA gives a 1.1- and 0.1-eV gap for the δ phase and β phase, respectively, both in a good agreement with Sahu *et al.*[19] However, the HSE06 functional widens the gaps to 2.0 and 0.9 eV for the two phases. For tetragonal H-tantala, GGA predicts a metallic system whereas HSE06 opens a gap of 0.9 eV, a substantial improvement over the GGA results [Fig. 3(c)]. GGA with VCA shows metallic property for tetragonal H-tantala, which is the same as O rich [Fig. 3(d)]. Since we currently do not have a VCA potential suitable for use with the HSE06 hybrid functional, and construction and testing of such a potential would constitute a major separate effort, we do not have DOS information on the 77-atom low-T systems [Fig. 3(e)].

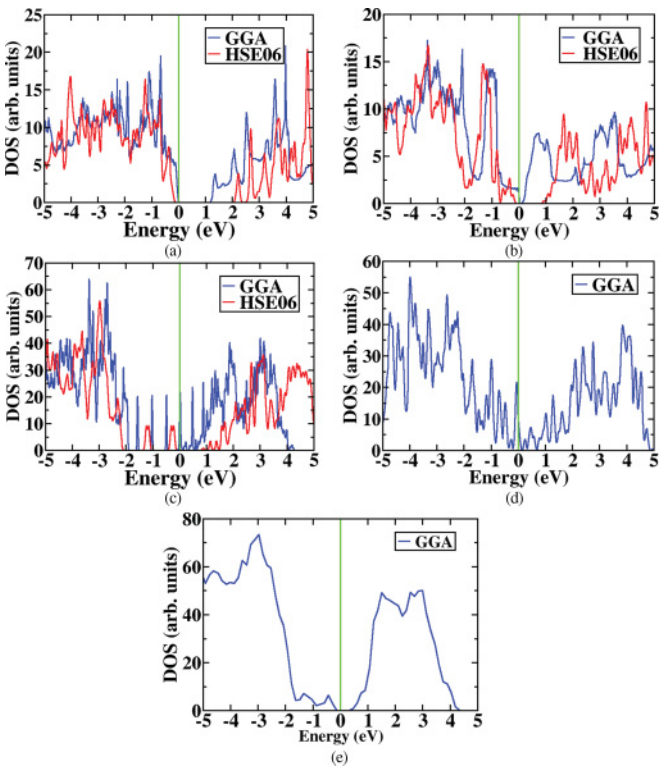

FIG. 3. (Color online) (a) DOS of δ-Ta_2O_5. (b) DOS of β-Ta_2O_5. (c) DOS of tetragonal H-Ta_2O_5. (d) DOS of tetragonal H-Ta_2O_5 with VCA. (e) DOS of low temperature 77 atoms. GGA is in blue and HSE06 is in red. Green lines indicate the Fermi level, which is adjusted to be zero.

C. Elastic moduli

In this section, we discuss the mechanical properties of Ta_2O_5 models. Our focus is on the elastic moduli, including bulk modulus, Young's modulus, and Poisson's ratio. All of the calculations started with the equilibrium states for the Ta_2O_5 structures.

Table III presents elastic tensors and derived mechanical functions using Eqs. (3)–(13). Because of symmetry, the number of independent elements varies from system to system. In this case, we remove symmetry constraints and allow all six distortions for every system. Based on the elastic tensors thus obtained, the symmetry is basically maintained in our calculation, though some small deviations exist. For example, c_{11} and c_{22} are different by 5 GPa for O-rich H-Ta_2O_5. All elements of the elastic tensor are taken into the calculation of elastic constants, which effectively is an average of those elements corresponding to symmetry. Our calculations show that the lower and upper limit of the shear modulus, G_R and G_V, from all systems range 49–97 GPa, and those of the bulk moduli range 105–221 GPa, Young's moduli 152–233 GPa, and Poisson's ratio 0.25–0.34. We take this as an indication that these crystals have moderately similar mechanical properties when averaged over all directions. It can be seen that the H-Ta_2O_5 (both for the O-rich and VCA model) has higher elastic moduli and Poisson's ratio than the three L-Ta_2O_5 structures, indicating that H-Ta_2O_5 is stiffer. The VCA makes tetragonal H-Ta_2O_5 have a higher shear modulus and Young's modulus than the O-rich model, but a lower bulk modulus. Among the three L-Ta_2O_5 crystalline structures, hexagonal δ-Ta_2O_5 shows lower moduli and Possion's ratio than the other two. The last three rows in Table III are Young's moduli along the x, y, and z directions, respectively. We will compare Y_z with a direct approach below.

D. Technical remarks: VCA and direct approach

In the direct approach, the conventional way to compute the bulk modulus using first-principles calculations is via Eq. (11). The volume change for each Ta_2O_5 structure discussed above was achieved by changing the lattice constants. For the two L-Ta_2O_5 of small unit cells, all of the atoms were allowed to relax in the cells with the selected volumes, while for all large systems the internal coordinates scale proportionally to the changes in lattice constants. The O-rich H-Ta_2O_5 is found to have the largest bulk modulus, 246 GPa (Table IV). All other vacancy-doped tetragonal H-Ta_2O_5 models, including defect_1, defect_2, and VCA, are calculated to be 217–227 GPa. Both moduli of two L-Ta_2O_5 structures are nearly the same values (228 and 223 GPa), which are quite close to those reported by Sahu *et al.*[19] However, they are quite different from the values obtained from the elastic tensor, especially in the case of the δ phase (108 GPa). A possible explanation for the discrepancy is that relaxation of the shape could lower the bulk modulus, whereas we do not let the unit-cell shape relax in our calculation. The bulk modulus of amorphous model is 234 GPa and lowest bulk modulus is 163 GPa for the amorphous VCA model.

TABLE III. Elastic constants, bulk moduli, shear moduli, Young's moduli, and Poisson's ratio of different phases of Ta_2O_5. Y_x, Y_y, and Y_z are Young's modulus along a, b, and c axes.

	Orthorhombic β-Ta_2O_5 (GPa)	Hexagonal δ-Ta_2O_5 (GPa)	Tetragonal O-rich (GPa)	Tetragonal_VCA (GPa)	Orthorhombic 77 atoms L-Ta_2O_5 (GPa)
c_{11}	290	175	379	445	224
c_{12}	126	104	173	67	106
c_{13}	52	169	131	130	44
c_{22}	263	167	374	443	256
c_{23}	115	3	130	132	42
c_{33}	428	403	366	326	430
c_{44}	78	47	65	64	51
c_{55}	39	46	65	64	54
c_{66}	52	57	62	62	36
G_R	64	49	77	81	57
G_V	80	72	84	97	76
B_R	171	105	221	207	140
B_V	174	110	221	208	144
Y	189	152	215	233	172
ν	0.32	0.26	0.34	0.34	0.30
Y_x	229	108	283	392	179
Y_y	188	97	280	389	204
Y_z	378	398	304	259	418

Direct calculation of Young's modulus involves much more effort compared to the bulk modulus. We focus only on the (001) direction for all systems for comparison with values listed in Table III (Y_z). To determine the ratio of tensile stress over tensile strain, we have elongated and compressed the lattice parameter c. For all systems, Young's moduli have been calculated statically. Our calculation shows that high Young's modulus (667 GPa for δ phase and 606 GPa for β phase) is a characteristic of the two L-Ta_2O_5 crystals. These values are much higher than the Y_z (398 GPa for δ phase and 378 GPa for β phase), which is caused by relaxation of internal coordinates. The high Y values suggest that (001) is a very stiff direction, which is consistent with results in Table III. The H-Ta_2O_5 structures show relatively lower Young's moduli than L-Ta_2O_5 and agree well with Table III. A range of values has been obtained for tetragonal H-Ta_2O_5 models. The O-rich system has a value of 430 GPa, while the two specific vacancy-doped models have 360 and 380 GPa, respectively. Young's modulus H-Ta_2O_5 with VCA is obtained as 345 GPa. The calculated Young's modulus of the amorphous phase is ~320 GPa, which is much higher than the experimentally measured 140 GPa (no amorphous phase calculated in Table III). Our results suggest that the amorphous VCA model may be useful for systematically approaching the experimental value. Based on our calculation, oxygen vacancies and disorder in crystals cause the materials to soften.

Finally, Poisson's ratios, the ratio of transverse contraction strain to axial extension strain, of these systems, has been computed. As seen in Table II, the values of Poisson's ratios in the (001) direction range from 0.09 to 0.23 in the low- and high-temperature crystalline phases, which are lower compared to polycrystalline-averaged values. Poisson's ratio of the amorphous system is determined as 0.27. Note that the Poisson ratios calculated directly are in the z direction, so it can be possible that the value is lower than the values in Table III. The amorphous system with oxygen defects described by the VCA structure has a Poisson's ratio of 0.20. The experimental value of 0.23 lies between 0.20 and 0.27, suggesting that fine tuning the amorphous-VCA model can possibly improve the agreement between theory and experiment.

Since results from VCA and explicit defect models yield similar mechanical properties as listed in Table IV, the VCA seems to be a good approach for modeling vacancies. However, the values from the direct approach are quite different from the ones obtained by using Eqs. (2)–(10). The reason is the constraints applied during calculations: For example, uniform lattice scaling in all directions is used for bulk modulus calculations, and fixed angles (among three lattice vectors) are assumed when loading the strain in one direction for calculating Young's modulus. These constraints lead to inaccurate numbers for systems as sensitive as Ta_2O_5.

IV. SUMMARY

In conclusion, the calculated mechanical properties of tantalum peroxide systems show that the Ta_2O_5 crystalline

TABLE IV. Bulk moduli, Young's moduli, and Poisson's ratio of different phases of Ta_2O_5. Y's are the Young's modulus along the c axis, calculated via direct method for validating VCA.

	B (GPa)	Y (GPa)	ν
Exp. (amorphous thin film)		140	0.23
O-rich H-Ta_2O_5	246	430	0.23
With VCA	224	345	0.22
Defect_1	217	360	0.23
Defect_2	227	380	0.23
168-atom amorphous	234	320	0.27
With VCA	163	263	0.20

polymorphs, and its derivatives have similar mechanical properties but are highly anisotropic. The (001) direction of the high-temperature phase is rather soft compared to all three low-temperature phases, but the (100) and (010) directions are stiffer. All L-Ta_2O_5 phases are energetically more stable than the H-Ta_2O_5 and the amorphous phases. In systems such as H-Ta_2O_5, 77-atom orthorhombic L-Ta_2O_5, and the amorphous structure, oxygen vacancies (or partial occupancy) soften the materials and lower the cohesive energy. Mass density and Young's modulus also decrease when the systems have oxygen vacancies. By comparison with experimental data, we conclude that the amorphous structure with oxygen vacancy is a good structural model for investigation of a Ta_2O_5 thin film, but a thorough investigation is needed in future studies. We also suggest that more experimental measurements should be carried out to understand various crystalline phases.

ACKNOWLEDGMENT

The authors would like to thank Prof. Samuel Trickey for discussion. The authors acknowledge the NSF/DMR and NSF/PHY for financial support, as well as DOE/NERSC and UF-HPC for computational resources.

[1] C. Chaneliere, J. L. Autran, R. A. B. Devine, and B. Balland, Mater. Sci. Eng. R **22**, 269 (1998).
[2] S. Zaima, T. Furuta, Y. Koide, Y. Yasuda, and M. Lida, J. Electrochem. Soc. **137**, 2876 (1990).
[3] H. Shinriki and M. Nakata, IEEE Trans. Electron Devices **38**, 455 (1991).
[4] Y. Nishioka, S. Kimura, H. Shinriki, and K. Mukai, J. Electrochem. Soc. **134**, 410 (1987).
[5] Y. Nakagawa and T. Okada, J. Appl. Phys. **68**, 556 (1990).
[6] Y. L. Zhou, M. Niinomi, T. Akahori, H. Fukui, and H. Toda, Mater. Sci. Eng. A **398**, 28 (2005).
[7] D. R. M. Crooks, P. Sneddon, G. Cagnoli, J. Hough, S. Rowan, M. M. Fejer, E. Gustafson, R. Route, N. Nakagawa, D. Coyne, G. M. Harry, and A. M. Gretarsson, Classical Quantum Gravity **19**, 883 (2002).
[8] D. R. M. Crooks, P. Sneddon, G. Cagnoli, J. Hough, S. Rowan, M. M. Fejer, E. Gustafson, R. Route, N. Nakagawa, D. Coyne, G. M. Harry, and A. M. Gretarsson, Classical Quantum Gravity **19**, 4229 (2002).
[9] S. D. Penn, P. H. Sneddon, H. Armandula, J. C. Betzwieser, G. Cagnoli, J. Camp, D. R. M. Crooks, M. M. Fejer, A. M. Gretarsson, G. M. Harry, J. Hough, S. E. Kittelberger, M. J. Mortonson, R. Route, S. Rowan, and C. C. Vassiliou, Classical Quantum Gravity **20**, 2917 (2003).
[10] A. Reisman, F. Holtzberg, M. Berkenblit, and M. Berry, J. Am. Chem. Soc. **78**, 4514 (1956).
[11] L. A. Aleshina and S. V. Loginova, Crystallogr. Rep. **47**, 415 (2002).
[12] C. Askeljung, B. O. Marinder, and M. Sundberg, J. Solid State Chem. **176**, 250 (2003).
[13] B. O. Marinder, J. Solid State Chem. **160**, 62 (2001).
[14] R. S. Roth and J. L. Waring, J. Res. Natl. Bur. Stand. Sect. A **74**, 485 (1970).
[15] R. S. Roth, J. L. Waring, and W. S. Brower, J. Res. Natl. Bur. Stand. Sect. A **74**, 477 (1970).
[16] N. C. Stephenson and R. S. Roth, Acta Crystallogr. Sect. B **27**, 1010 (1971).
[17] J. L. Waring and R. S. Roth, J. Res. Natl. Bur. Stand. Sect. A **72**, 175 (1968).
[18] H. Kimura, J. Mizuki, S. Kamiyama, and H. Suzuki, Appl. Phys. Lett. **66**, 2209 (1995).
[19] B. R. Sahu and L. Kleinman, Phys. Rev. B **69**, 165202 (2004).
[20] G. S. Oehrlein, F. M. Dheurle, and A. Reisman, J. Appl. Phys. **55**, 3715 (1984).
[21] A. Fukumoto and K. Miwa, Phys. Rev. B **55**, 11155 (1997).
[22] W. Andreoni and C. A. Pignedoli, Appl. Phys. Lett. **96**, 062901 (2010).
[23] S. Lagergren and A. Magneli, Acta Chem. Scand. **6**, 444 (1952).
[24] F. Laves and W. Petter, Helv. Phys. Acta **37**, 617 (1964).
[25] X. Q. Liu, X. D. Han, Z. Zhang, L. F. Ji, and Y. J. Jiang, Acta Mater. **55**, 2385 (2007).
[26] D. Makovec, H. M. Zuo, R. Twesten, and D. A. Payne, J. Solid State Chem. **179**, 1782 (2006).
[27] L. Nordheim, Ann. Phys. **9**, 607 (1931).
[28] G. Kresse and J. Furthmuller, Phys. Rev. B **54**, 11169 (1996).
[29] G. Kresse and J. Furthmuller, Comput. Mater. Sci. **6**, 15 (1996).
[30] G. Kresse and J. Hafner, Phys. Rev. B **48**, 13115 (1993).
[31] W. Kohn and L. J. Sham, Phys. Rev. **140**, 1133 (1965).
[32] G. Kresse and D. Joubert, Phys. Rev. B **59**, 1758 (1999).
[33] P. E. Blochl, Phys. Rev. B **50**, 17953 (1994).
[34] J. P. Perdew and Y. Wang, Phys. Rev. B **45**, 13244 (1992).
[35] H. J. Monkhorst and J. D. Pack, Phys. Rev. B **13**, 5188 (1976).
[36] M. Methfessel and A. T. Paxton, Phys. Rev. B **40**, 3616 (1989).
[37] J. Paier, M. Marsman, K. Hummer, G. Kresse, I. C. Gerber, and J. G. Angyan, J. Chem. Phys. **124**, 154709 (2006).
[38] J. Heyd, G. E. Scuseria, and M. Ernzerhof, J. Chem. Phys. **118**, 8207 (2006).
[39] Y. Le Page and P. Saxe, Phys. Rev. B **65**, 104104 (2002).
[40] H. Z. Yao, L. Z. Ouyang, and W. Y. Ching, J. Am. Ceram. Soc. **90**, 3194 (2007).
[41] P. Ravindran, L. Fast, P. A. Korzhavyi, B. Johansson, J. Wills, and O. Eriksson, J. Appl. Phys. **84**, 4891 (1998).
[42] W. Voigt, *Lehrbuch der kristallphysik* (Teubner, Leipzig, 1928).
[43] A. Reuss and Z. Angew, J. Appl. Math. Mech./Z. Angew. Math. Mech. **9**, 49 (1929).
[44] R. Hill, Proc. Phys. Soc. London Sect. A **65**, 349 (1952).
[45] J. F. Nye, *Physical Properties of Crystals: Their Representation by Tensors and Matrices* (Oxford University Press, Oxford, UK, 1985).
[46] R. Bassiri, K. B. Borisenko, D. J. H. Cockayne, J. Hough, I. MacLaren, and S. Rowan (unpublished).